Enhanced electrical spin injection and detection in biased lateral ferromagnet–semiconductor structures

2007 J. Phys.: Condens. Matter 19 276201

(http://iopscience.iop.org/0953-8984/19/27/276201)

IOP PUBLISHING JOURNAL OF PHYSICS: CONDENSED MATTER

J. Phys.: Condens. Matter **19** (2007) 276201 (19pp) doi:10.1088/0953-8984/19/27/276201

Enhanced electrical spin injection and detection in biased lateral ferromagnet–semiconductor structures

J J H M Schoonus, A T Filip, H J M Swagten and B Koopmans

Department of Applied Physics, Center for NanoMaterials (cNM) and COBRA Research Institute, Eindhoven University of Technology, PO Box 513, 5600MB Eindhoven, The Netherlands

E-mail: j.j.h.m.schoonus@tue.nl

Received 15 November 2006, in final form 30 May 2007
Published 20 June 2007
Online at stacks.iop.org/JPhysCM/19/276201

Abstract

The realization of a fully electrical semiconductor-based device making use of the electron spin is of fundamental importance for physically studying spin-related phenomena. We have performed a detailed theoretical analysis of the feasibility of all electrical spin injection and detection in semiconductors by means of ferromagnetic electrodes and including spin-selective interface barriers to overcome the impedance mismatch. Based on the Poisson and diffusion equation, including electric field effects, the expected resistance difference for parallel and anti-parallel configurations of the ferromagnetic electrodes is analytically calculated and the influence of the sample and measurement geometry is extensively investigated. In this paper, we propose a new measurement geometry, for which we predict a clearly larger spin accumulation over a larger distance. Electric fields created in different sample regions via extra bias voltages will compensate spin loss in side branches. Even when the spin diffusion length is orders of magnitude smaller than the semiconductor length, the magnetoresistance in lateral devices closely approaches values for vertical devices.

1. Introduction

The research to exploit the spin degree of freedom in semiconductors has gained a lot of momentum recently [1], fuelled by potential applications in the field of quantum computation [2], magnetic field sensors, memory and logic devices [3]. Semiconductors are attractive because of their nonlinear behaviour, the controllability of the impedance via doping, and their long spin relaxation times. Best established in the field is the optical control of spins in semiconductors. Optical injection and detection in spin-polarized carriers are used to study spin diffusion and spin transport across semiconducting interfaces [4]. Efficient electrical injection of spin-polarized currents in a III–V semiconductor has been proven from either a dilute magnetic semiconductor [5], a metallic ferromagnetic material [6], or across AlO_x

tunnel barriers [7]. Electrical spin injection and accumulation, subject to electric, magnetic and strain fields, was optically imaged in a GaAs channel of lateral spin-transport devices [8, 9]. Recently, a demonstration of a fully electrical scheme for achieving spin injection, transport and detection in a single device was given by Lou *et al* [10]. Although the bias dependence of the nonlocal signal and the spin polarization is not completely understood, they showed irrefutable proof using the Hanle effect. A transverse magnetic field suppresses the nonlocal signal at the detection contact by inducing spin precession and dephasing in the channel. Achieving a fully electrical semiconductor-based device that makes use of the electron spin is of fundamental importance for physically studying spin-related phenomena. For the design and fabrication of such a device a comprehensive theoretical understanding of spin injection and spin transport in semiconductors is necessary, and qualitative, usable design rules are given in this paper.

From a theoretical point of view, Johnson and Silsbee introduced a concept based on spin-dependent distribution functions to describe the spin transport for an interface between ferromagnetic and nonmagnetic metals [11]. Valet and Fert [12] extended the model in a Boltzmann equation formalism, that reduces to the same macroscopic transport equations if the mean free path is much shorter than the spin diffusion length. Recently, numerical studies in perpendicular-transport structures verified that their approach is also valid in the limit of a spin diffusion length comparable to the appropriate mean free path [13]. These macroscopic transport equations were utilized to analyse the feasibility of spin injection into semiconductors [14] and, recently, also organic systems [15]. The results showed that the crucial parameter is the resistance mismatch between semiconductor and metal. One potential solution was suggested by Rashba [16]: one could make use of tunnelling as injection mechanism. The conditions for efficient spin injection from a ferromagnetic metal into a semiconductor were established by Fert and Jaffrès [17] and the magnetoresistance of a ferromagnet–semiconductor–ferromagnet trilayer was computed [18–20]. Several devices using lateral semiconductor spin-valves with novel bias schemes, like spin transference and magnetoresistance amplification in a transistor [21], and electric readout of magnetization dynamics in a ferromagnet–semiconductor system [22] are proposed. Another interesting scheme was studied by McGuire *et al* [23], who calculated the lateral spin transport induced by ferromagnetic proximity on a two-dimensional electron gas.

In contrast with metals, for which the electric field is essentially screened, in semiconductors a moderate electric field can dominate the carrier motion. Yu and Flatté [24] examined the spin diffusion in lightly doped semiconductors by consistently taking into account electric-field effects and nondegenerate electron statistics. For high fields, spin transport is described in terms of two field-induced spin diffusion lengths. D'Amico [25] analysed the spin transport in semiconductors in the intermediate to degenerate regime.

For the development of electrical semiconductor spintronic devices, self-consistent two-dimensional charge transport simulations, taking into account tunnelling, Fermi-level pinning, band bending, impact ionization and their bias dependence, are a necessity. Although considerable progress in this direction has been witnessed in recent years [26], it is crucial to realize that the basic transport behaviour of realistic devices has not been documented in much detail. More specifically, the effect of elementary parameters on the magnetoresistance, such as the electric field, spin diffusion length, the resistance of the electrodes, interface barriers and semiconductor, is intimately related to the geometry of the semiconductor channel and the adjacent entities for injection and detection, and should be carefully analysed.

In this paper, we calculate the magnetoresistance of a vertical sample layout, consisting of a ferromagnetic metal–nonmagnetic semiconductor–ferromagnetic metal stack with spin-selective (semi-)insulating barriers, as well as of a lateral layout, with two metallic ferromagnetic electrodes on top of a planar nonmagnetic semiconductor channel, also

separated by spin-selective interface layers. Our study is in particular aimed at n-doped semiconductors, where the spin diffusion lengths are extremely long, possibly leading to very large magnetoresistance [8]. Generally, a Schottky barrier will form at the interfaces of the insulating layer and the semiconductor, leading to positively charged donor ions left behind in the depletion region that is practically stripped of electrons. Although injection of electrons is feasible when a voltage is applied across such a device, the presence of the Schottky barrier prevents tunnelling into the detector electrode in the reversed bias. However, by highly doping the region just beneath the semiconductor surface [8, 26, 27], numerical simulations show that the width of the Schottky barrier is much smaller than the spin flip length and comparable to the width of the insulating barrier resistance [28, 29]. Therefore, it only affects electron transport across the barrier, i.e. it renormalizes the interface barrier resistance, but is does not affect the bulk transport properties. In this regime, we can assume there is no space charge in the semiconductor, especially near the interface with the spin-selective barrier, and the electron density is constant throughout the nonmagnetic semiconductor. In other words, we assume that the bottom of the conduction band remains substantially flat in the vicinity of the interface on a length scale comparable to the spin flip length. Therefore, we can use the drift–diffusion equation, which assumes charge neutrality throughout our layered structure. Furthermore, this work may assist in the understanding of spin transport in MnAs/GaAs lateral spin-valves [30], where also local changes in band structure and carrier density are negligible as these are not taken into consideration in our calculation. We would like to emphasize that our theory clearly not applies for spin injection via (Zn, Mn, Be)Se as the dilute magnetic semiconductor into the nonmagnetic semiconductor (Zn, Be)Se. For voltage drops across the interface larger than a few mV, Schmidt *et al* [31] calculated for this case that the spin-injection efficiency decreases strongly. The effect in this nonlinear regime is caused by repopulation of the minority spin level in the magnetic semiconductor due to band bending at the interface. Vanheertum *et al* [32] pointed out that special care has to be taken concerning the width of the contacts to avoid depolarization of the carriers caused by parallel current flow in the highly doped region directly underneath the electrode. Therefore, we assume single point contacts in our analysis, corresponding to direct perpendicular injection in the semiconductor and thus negligible current flow in the suppression layer parallel to the electrode.

Based on the assumption of charge neutrality, we derive an analytical expression for the magnetoresistance and examine the role of the interface resistances and spin diffusion length for different realistic sample geometries. It will be illustrated that the electric field effect can considerably enhance the magnetoresistance as long as the spin-selective interfacial barriers are perfectly matched. To eliminate the detrimental effect of the electric field in the semiconductor side branches on the magnetoresistance, an alternative measurement geometry is introduced in which we apply, in addition to the ac measurement signal, an extra dc bias voltage over the semiconductor to tune the electric field in the semiconductor. In this way, the magnetoresistance for lateral devices can increase to values which are normally found for standard vertical trilayer devices.

2. Spin-polarized transport in semiconductors

As reported by Yu and Flatté [24], spin transport in lightly doped semiconductors can be described by a drift–diffusion equation by consistently taking into account electric field effects and nondegenerate electron statistics. In this section, their main results for a better understanding of the next section will be summarized, we discuss the validity for (non)magnetic metals and GaAs, and we introduce the parameters used throughout this paper.

We consider here a n-doped homogeneous system without space charge. For a current density flowing in the x direction, a one-dimensional solution for the Poisson and diffusion

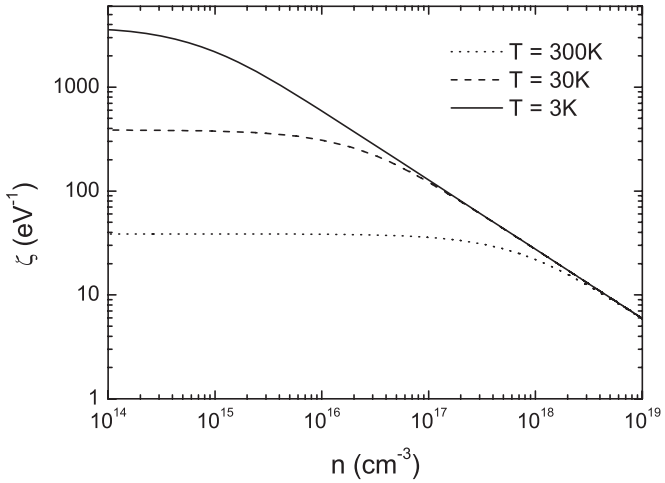

Figure 1. ζ as a function of the electron density for different temperatures in three-dimensional systems. The effective electron mass is 0.065 m_0, where m_0 is the free electron mass.

equation is searched in terms of the electrochemical potential $\bar{\mu}_{\uparrow}(x) = \mu_{\uparrow}(x) - eV(x)$ for spin up and spin down [33], respectively:

$$\frac{\partial^2 \bar{\mu}_{\uparrow(\downarrow)}}{\partial x^2} - \frac{1}{2}\zeta_{\uparrow(\downarrow)} eE \frac{\partial \bar{\mu}_{\uparrow(\downarrow)}}{\partial x} = \frac{(\bar{\mu}_{\uparrow(\downarrow)} - \bar{\mu}_{\downarrow(\uparrow)})}{\lambda^2_{\uparrow(\downarrow)}}, \tag{1}$$

with

$$\zeta_{\uparrow(\downarrow)} = \frac{\int_0^\infty N_{\uparrow(\downarrow)}(\epsilon - \epsilon_{c\uparrow(\downarrow)}) \frac{\partial f}{\partial \epsilon} \, \mathrm{d}\epsilon}{\int_0^\infty N_{\uparrow(\downarrow)}(\epsilon - \epsilon_{c\uparrow(\downarrow)}) f \, \mathrm{d}\epsilon}, \tag{2}$$

where E is the electric field, N is the density of states, f the Fermi–Dirac distribution function and $-e$ and $\epsilon_{(c)}$ are respectively the charge and energy (at the conduction band) of the electrons.

The bias regime for which the electrical field effects dominates depends on the relative magnitude of the drift and the diffusive term. In the drift term, ζ expresses the influence of the temperature and doping. For three temperatures, ζ is plotted in figure 1 as a function of the electron density n. The metal regime is characterized by a density of conducting electrons higher than 1×10^{18} cm^{-3}, and a critical electric field, where the drift term starts dominating the diffusive term, is independent of temperature. The density of states varies only slightly with the energy at the Fermi level and the numerator of equation (2) becomes constant and thus independent of the temperature. For intermediate and lightly doped semiconductor spintronic devices, at temperatures down to 30 K, a moderate electric field can already dominate the carrier motion [34] and the drift term cannot be neglected any longer. However, in the degenerated regime where the Fermi energy is much smaller than the thermal energy, for GaAs estimated by $T < 4.5 \ln(n/10^{14}\ \mathrm{cm}^{-3})$ with n in cm^{-3} and T in K, carrier–carrier interactions assume a relevant role [35] and they partly weaken the electric field effects. As a result, higher applied fields are necessary for a significant contribution of the drift term. Only for lightly doped semiconductors ($n < 1 \times 10^{16}$ cm^{-3}) and temperatures above 3 K, will the results of equation (1) be reasonably accurate.

For nonmagnetic materials or materials with low spin polarization, the bottom edge of the conduction band is approximately equal for both spin species, and $\zeta_{\uparrow}$ can be set equal to $\zeta_{\downarrow}$. For ferromagnetic materials, $\zeta_{\uparrow}$ differs from $\zeta_{\downarrow}$. Via the Einstein equation ζ is equal

to the mobility divided by the diffusion constant and the electron charge. The mobility and diffusion constant of the lower-conductivity spin species are dominant and dependent on the spin polarization of the material equations, and we could mathematically solve equation (1) for $\bar{\mu}_\uparrow$ and $\bar{\mu}_\downarrow$. However, for simplicity we neglect, analogously to nonmagnetic materials, the spin difference in ζ, which makes the analysis only accurate for low-polarized materials. We assume that conductivity predominantly takes place at the Fermi level and introduce a spin-dependent conductivity times channel area (width times height) σ. The general form of the steady-state solution to equation (1) in a homogeneous medium, using the requirement of particle and current conservation, is given by

$$\mu_\uparrow = A + Bx + \frac{C}{\sigma_\uparrow}\exp(-x/\lambda_\mathrm{d}) + \frac{D}{\sigma_\uparrow}\exp(x/\lambda_\mathrm{u}) \tag{3a}$$

$$\mu_\downarrow = A + Bx - \frac{C}{\sigma_\downarrow}\exp(-x/\lambda_\mathrm{d}) - \frac{D}{\sigma_\downarrow}\exp(x/\lambda_\mathrm{u}), \tag{3b}$$

where $\sigma_{\uparrow(\downarrow)}$ is the conductivity times channel area of the spin-up(down) channel. The two quantities λ_u and λ_d are the upstream and downstream spin diffusion lengths [33], defined as

$$\lambda_\mathrm{d} = \frac{1}{\lambda}\left(-\frac{M}{2} + \sqrt{\left(\frac{M}{2}\right)^2 + 1}\right)^{-1} \tag{4a}$$

$$\lambda_\mathrm{u} = \frac{1}{\lambda}\left(+\frac{M}{2} + \sqrt{\left(\frac{M}{2}\right)^2 + 1}\right)^{-1}, \tag{4b}$$

with

$$M = \zeta e E \lambda, \tag{5}$$

where M is defined as a dimensionless parameter characterizing the ratio between the electrostatic energy and thermal energy, and $(1/\lambda)^2 = (1/\lambda_\downarrow)^2 + (1/\lambda_\uparrow)^2$. In metals, $M \ll 1$ and the drift term in equation (1) can be neglected, because the effective electric field is screened by the individual Coulomb fields of all the conducting electrons. However, for semiconductors, M can be significantly larger than 1. For example in GaAs, with a doping of 1×10^{16} cm^{-3}, a spin diffusion length of 2 μm [36], and an applied voltage of 10 mV, M could be already of the order of 100. The spin diffusion length of electrons moving oppositely to the applied field is increased, while the spin diffusion length of electrons moving in the direction of the field is decreased. In addition to a random diffusive walk, the electrons follow a drift motion in the direction of the field [33].

To summarize this part, an analytical drift–diffusion equation is given for ferromagnetic metals, nondegenerate semiconductors and, in first order, for degenerate nonmagnetic semiconductors. We have discussed the validity for GaAs related to the carrier density, polarization and temperature. In the next section, using the drift–diffusion equation, the combined effects of interface barriers, semiconductor resistance, spin diffusion length and applied electric field will be studied in realistic device and measurement geometries.

3. Magnetoresistance calculations

We apply the macroscopic spin transport model for two geometries using a system composed of a ferromagnet–interface barrier–semiconductor–interface barrier–ferromagnet, as schematically shown in figure 2. By an interface barrier, we mean a spin-selective (semi-) insulating layer to overcome the impedance mismatch, and this practically implies the presence of a Schottky barrier or thin insulating barrier. As explained in the introduction, the Schottky

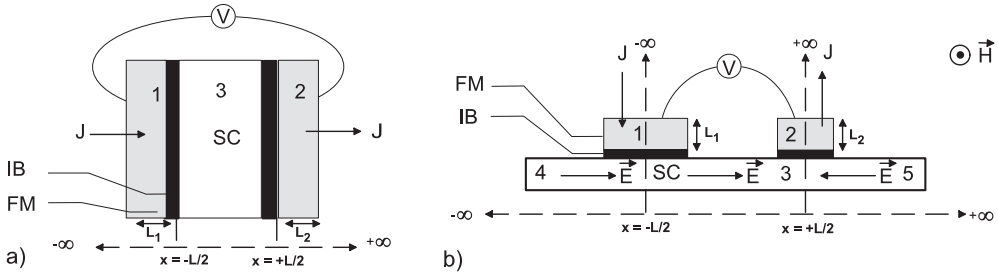

Figure 2. (a) Vertical ferromagnet–interface barrier–semiconductor–interface barrier–ferromagnet geometry. (b) Lateral ferromagnet–interface barrier–semiconductor–interface barrier–ferromagnet geometry. Numerals and axis indications refer to regions where separate solutions of the diffusion equation are considered. Current is injected in region 1 and extracted from region 2, while the voltage is measured between the same regions. Arrows indicate the direction of the electric field in the lateral device.

barrier at the interface of the semiconductor and insulator is suppressed by highly doping the region just beneath the semiconductor surface. This enables effective spin injection and detection in the semiconductor and allows that the calculations can be performed with the assumptions of homogeneous systems and local charge neutrality. The first geometry, as discussed in the literature [37], we denote as a vertical geometry (see figure 2(a)). The lateral geometry shown in figure 2(b) differs from the standard vertical geometry, in particular due to the semiconductor channel that extends to infinity in both directions, and the two electrodes are grown on top at a mutual distance L. Note that an epitaxially grown lateral semiconductor device is technologically more easily realizable; in addition, it allows for four terminal measurements. However, the two side branches act as an extra channel for spin loss. Therefore, the magnetoresistances in the lateral device is expected to be lower in comparison with a vertical device, which will be further analysed below.

First, we will solve the drift–diffusion equation in each region and for each spin state of the vertical geometry. Three different regions can be identified: region 1 is the ferromagnetic injector, region 2 is the ferromagnetic detector, and region 3 is the semiconductor. The parameters used are labelled with a subscript referring to these region numbers. Current is injected in region 1 and extracted in region 3, and the voltage is measured between regions 1 and 3. Two configurations can occur: parallel magnetization and antiparallel magnetization of the electrodes. We will first consider parallel configuration of the ferromagnetic electrodes. The chemical potentials have the general form like equations (3*a*) and (3*b*) and are for region 1, 2 and 3:

$$1 : \mu_{\uparrow(\downarrow)} = A_{\mathrm{p}} + \frac{Je}{\sigma_{1f}}x \pm \frac{B_{\mathrm{p}}}{\sigma_{1\uparrow(\downarrow)}}\exp(x/\lambda_f) \tag{6a}$$

$$2 : \mu_{\uparrow(\downarrow)} = C_{\mathrm{p}} + \frac{Je}{\sigma_{2f}}x \pm \frac{D_{\mathrm{p}}}{\sigma_{2\uparrow(\downarrow)}}\exp(-x/\lambda_f) \tag{6b}$$

$$3 : \mu_{\uparrow(\downarrow)} = \frac{Je}{\sigma_3}x \pm \frac{2F_{\mathrm{p}}}{\sigma_3}\exp(-x/\lambda_{\mathrm{d}}) \pm \frac{2G_{\mathrm{p}}}{\sigma_3}\exp(x/\lambda_{\mathrm{u}}). \tag{6c}$$

We have written for the total conductivity of the ferromagnet $\sigma_{1(2)f} = \sigma_{1(2)\uparrow} + \sigma_{1(2)\downarrow}$ and for the total current density $J = J_\uparrow + J_\downarrow$. A_{p}, B_{p}, C_{p}, D_{p}, F_{p} and G_{p} are six independent unknown constants. For regions 1 and 2, the exponential terms which increase to infinite for $x \to \pm\infty$, respectively, are omitted, because no spin splitting is assumed in the electrode far away from the interface barrier. The linear term in equations (6*a*)–(6*c*) is required due to the condition that at

$\pm\infty$ the solutions for the chemical potentials must coincide with the standard bulk dependence ($\mu_\uparrow|_{x\to\pm\infty} = \mu_\downarrow|_{x\to\pm\infty} = H + Je/\sigma \cdot x$), with H a constant. The average potential at the middle of the semiconductor is set to zero. Finally, because of particle conservation, the equations for the spin-down electrons can be found by putting a minus sign in front of constants B_p, D_p, F_p and G_p and adjusting the conductivity for the negative spin species.

If no spin flip scattering at the interface with the interface barrier is present, the first boundary condition at the interfaces is the discontinuity of $\mu_\uparrow$ and $\mu_\downarrow$. This is associated with the existence of spin-selective injector and detector interface resistances $R_\mathrm{ib}/(1+(-)P_0)$, that is,

$$\mu_{\uparrow(\downarrow)(x=-\frac{L}{2}^-)} - \mu_{\uparrow(\downarrow)(x=-\frac{L}{2}^+)} = \frac{2R_\mathrm{ib1}}{(1+(-)P_0)} J_{\uparrow(\downarrow)} \tag{7a}$$

$$\mu_{\uparrow(\downarrow)(x=-+\frac{L}{2}^-)} - \mu_{\uparrow(\downarrow)(x=+\frac{L}{2}^+)} = \frac{2R_\mathrm{ib2}}{(1+(-)P_0)} J_{\uparrow(\downarrow)}, \tag{7b}$$

where $J_{\uparrow(\downarrow)}$ is the current in the spin-up(down) channel and P_0 is the polarization at the interface between the ferromagnetic layer and the barrier. Secondly, the current density in each spin channel has to be conserved:

$$J_{\uparrow(\downarrow)}(x = L/2^-) = J_{\uparrow(\downarrow)}(x = L/2^+). \tag{8}$$

In total there are eight equations: two boundary conditions for two interfaces, one for each spin state. From this, the unknown constants of equations (6*a*)–(6*c*) can be calculated and the spatial dependence of the two spin potentials are determined relative to the equilibrium chemical potential.

Secondly, we consider that the magnetization orientation of the detection ferromagnetic electrode changes relative to the injection electrode. This is the situation of the antiparallel (ap) magnetization. This implies that $2R_\mathrm{ib2}/(1+P_0)$ should be exchanged for $2R_\mathrm{ib2}/(1-P_0)$ in equations (7*a*) and (7*b*), the constants A_p, B_p, C_p, D_p, F_p and G_p should be exchanged for A_ap, B_ap, C_ap, D_ap, F_ap and G_ap, and $\sigma_{2\uparrow(\downarrow)}$ should be exchanged for $\sigma_{2\downarrow(\uparrow)}$ in equation (6*a*), (6*b*) and (6*c*), because the minor (major) spin species in the injector electrode will be the major (minor) spin species in the detector electrode. The difference between constants $A_\mathrm{p(ap)}$ and $C_\mathrm{p(ap)}$ for the parallel (antiparallel) configuration equals the difference between the electrochemical potentials at both ferromagnetic ends. Because $A_\mathrm{p(ap)} - C_\mathrm{p(ap)}$ is proportional to J, the resistances for the parallel (R_p) (antiparallel (R_ap)) configuration follow directly from these two constants. The resistance change between parallel and antiparallel configurations of the magnetizations of the two electrodes, for a vertical geometry, can be calculated as

$$\frac{R_\mathrm{ap} - R_\mathrm{p}}{R_0} = 4\left(\frac{P_0 R_\mathrm{ib1}}{1-P_0^2} + \frac{P_1 R_1}{1-P_1^2}\right)\left(\frac{P_0 R_\mathrm{ib2}}{1-P_0^2} + \frac{P_2 R_2}{1-P_2^2}\right) \times \frac{1}{R_\mathrm{sc}(R_1 + R_\mathrm{ib1} + R_\mathrm{sc} + R_\mathrm{ib2} + R_2)} \times \frac{\left\{\frac{(M_3^2+4)^{1/2}}{K_3}\cosh\left(\frac{M_3}{2K_3}\right)\right\}}{\left\{(1+Q_4^+Q_2)(1+Q_3^+Q_1)\exp\left(\frac{(M_3^2+4)^{1/2}}{2K_3}\right) - (1+Q_4^-Q_2)(1+Q_3^-Q_1)\exp\left(-\frac{(M_3^2+4)^{1/2}}{2K_3}\right)\right\}}$$

with

$$
\begin{aligned}
Q_1 &= \left[\frac{R_{\mathrm{ib1}}}{1-P_0^2} + \frac{2R_1}{1-P_1^2}\frac{K_1}{M_1+\sqrt{M_1^2+4}}\right] \\
Q_2 &= \left[\frac{R_{\mathrm{ib2}}}{1-P_0^2} + \frac{2R_2}{1-P_2^2}\frac{K_2}{M_2+\sqrt{M_2^2+4}}\right] \\
Q_3^{\pm} &= \left[\frac{1}{K_3 R_{\mathrm{sc}}}\left(+\frac{M_3}{2} \pm \sqrt{\left(\frac{M_3}{2}\right)^2+1}\right)\right] \\
Q_4^{\pm} &= \left[\frac{1}{K_3 R_{\mathrm{sc}}}\left(-\frac{M_3}{2} \pm \sqrt{\left(\frac{M_3}{2}\right)^2+1}\right)\right],
\end{aligned}
\tag{9}
$$

where $P_{1(2)} = (\sigma_{1(2)\uparrow} - \sigma_{1(2)\downarrow})/\sigma_{1(2)f}$ is the bulk spin polarization of the injector and detector electrode, respectively, and $R_{1(2)} = L_{1(2)}/\sigma_{1(2)f}$ are the resistances of the two electrodes. $R_{\mathrm{sc}} = L/\sigma_s$ is the resistance of the semiconductor channel, L_1, L_2 and L are the lengths of ferromagnetic injector and detector electrodes and the semiconductor part between the two electrodes, respectively, and $K_1 = \lambda_1/L_1$, $K_2 = \lambda_2/L_2$ and $K_3 = \lambda/L$. The resistance difference is normalized by the sum of the spin-independent resistance $R_0 = R_1 + R_{\mathrm{ib1}} + R_{\mathrm{sc}} + R_{\mathrm{ib2}} + R_2$ instead of R_{p} to keep the expression compact. Using a resistor model, that includes spin-selective interface barriers and a spin diffusion length in the semiconductor, we checked that the difference between our magnetoresistance (equation (9)) and the regularly used $(R_{\mathrm{ap}} - R_{\mathrm{p}})/R_{\mathrm{p}}$, mainly proportional to P_0, is less than 2% for the calculated results in the following sections.

In the limit of small electric field, we checked that equation (9) converges to the all-metal regime as treated by Fert *et al* [17] and Jedema *et al* [38]. For small bulk spin polarizations, the magnetoresistance is quadratically proportional to the polarization, corresponding to the simple diffusive model of van Son *et al* [39].

We will now discuss the derivation of the magnetoresistance measured in a lateral geometry in which the semiconductor layer spreads from $-\infty$ to ∞ as can be seen from figure 2(b). At positions $x = -L/2$ and $L/2$ on the semiconductor two ferromagnetic electrodes are placed, separated from the semiconductor via an interface barrier. We assume that the width of the electrodes is negligibly small compared to the channel length, and therefore, the current is injected at only one specific point into the semiconductor. Furthermore, we assume no depth dependence of the current throughout the semiconductor channel. The conditions and equations for regions 1, 2 and 3 can be treated analogously to the vertical structure. However, for regions 4 and 5 the total current of both spin channels must be zero for $x = \pm\infty$, which leads to

$$
4 : \mu_{\uparrow(\downarrow)} = H \pm \frac{2N}{\sigma_s}\exp(x/\lambda_s) \tag{10a}
$$

$$
5 : \mu_{\uparrow(\downarrow)} = O \pm \frac{2R}{\sigma_s}\exp(-x/\lambda_s). \tag{10b}
$$

The five equations for the chemical potentials can be solved with boundary conditions analogously obtained as for the vertical structure (equations (7*a*) and (8)). Additionally, continuity is assumed of spin-up and spin-down chemical potentials and continuity of spin-up and spin-down currents between the two semiconductor regions at the injection and the detection point. The same general formula holds for the lateral local measurement geometry,

with the exception that $Q^{\pm}_{3(4)}$ is now defined as

$$Q_3^{\pm} = \left[\frac{1}{K_3 R_{\mathrm{sc}}}\left(+\frac{M_3}{2}+\frac{M_4}{2} \pm \sqrt{\left(\frac{M_3}{2}\right)^2+1}+\sqrt{\left(\frac{M_4}{2}\right)^2+1}\right)\right]$$
$$Q_4^{\pm} = \left[\frac{1}{K_3 R_{\mathrm{sc}}}\left(-\frac{M_3}{2}+\frac{M_5}{2} \pm \sqrt{\left(\frac{M_3}{2}\right)^2+1}+\sqrt{\left(\frac{M_5}{2}\right)^2+1}\right)\right]. \tag{11}$$

For the vertical as well as the lateral geometry, the spin flip length in low-polarized ferromagnetic metals and in absence of electric fields, is several orders of magnitude smaller than in a nonmagnetic semiconductor. Additionally, for both spin states the characteristic electrode resistance is much smaller than the interface resistances. Therefore, we neglect the dependence of the bulk ferromagnet properties on the magnetoresistance ($R_{1,2} = 0$), and the magnetoresistance becomes independent of the bulk spin polarizations in the ferromagnetic electrodes P_1 and P_2. The spin polarization depends, among other things, on material combinations and applied bias. In the following analysis the polarization at the interface P_0 will be fixed to 0.4, a conservative estimation of the injection systems for low bias: $P_0 = 0.4$ for Co/AlO_x [40], $P_0 = 0.57$ for CoFe/MgO [41], and $P_0 = 0.85$ for GaMnAs/Ga [42]. In the following subsections, we will use equations (9) and (11) to calculate the dependence of the magnetoresistance on the interface barrier resistances, the applied electric field and the spin diffusion length for the vertical and lateral geometry, as well as for a newly proposed geometry with additional electric biasing of the semiconductor branches.

3.1. Magnetoresistance of a vertical measurement geometry

In figure 3, the magnetoresistance is calculated for different values of the electric field, expressed by the parameter M (0, 40 and 100), as a function of the ratio between the interface barrier resistance and the resistance of the semiconductor, with $K_3 = \lambda/L = 5$. The figure is divided in three columns, showing the results for the vertical measurement geometry (column A), the lateral local measurement geometry (column B) and the newly proposed measurement geometry for which the semiconductor side branches are biased (column C). For the vertical geometry discussed here, the magnetoresistance is calculated with equation (9), where M_3 is defined as M. The results of column B and C will be discussed in sections 3.2 and 3.3.

If we focus on figure 3(A) for $M = 0$, a maximum in the magnetoresistance occurs for $R_{\mathrm{ib1}}/R_{\mathrm{sc}} = R_{\mathrm{ib2}}/R_{\mathrm{sc}} \approx 6.5$. Note that this value heavily depends on the chosen parameters, such as P_0 and λ/L. Contours mark the different regions for which the magnetoresistance is higher than 10%, 5%, 1% and 0.1%. The magnetoresistance is proportional to the spin splitting $(\mu_\uparrow - \mu_\downarrow)$ in the middle of the channel in the antiparallel configuration divided by the total voltage drop over the device [12]. For small $R_{\mathrm{ib}}/R_{\mathrm{sc}}$, the discontinuities in the chemical potential introduced by the interface resistances are too small to generate a high enough spin splitting in the semiconductor (in comparison with the splitting in the ferromagnet). As a result, the current will not be spin polarized and a low magnetoresistance is expected. This phenomenon is known as the impedance mismatch. In the region near the maximum magnetoresistance, the predominant contribution to the variation of electrochemical potential comes from the potential drops at the interface. In the antiparallel configuration, this gives rise to a spin splitting which is hardly affected by the spin flips in the semiconductor since the number of spin flips is much too small in comparison with the total amount of carriers. For high values of $R_{\mathrm{ib}}/R_{\mathrm{sc}}$ for the high-λ/L regime, the spin splitting saturates. However,

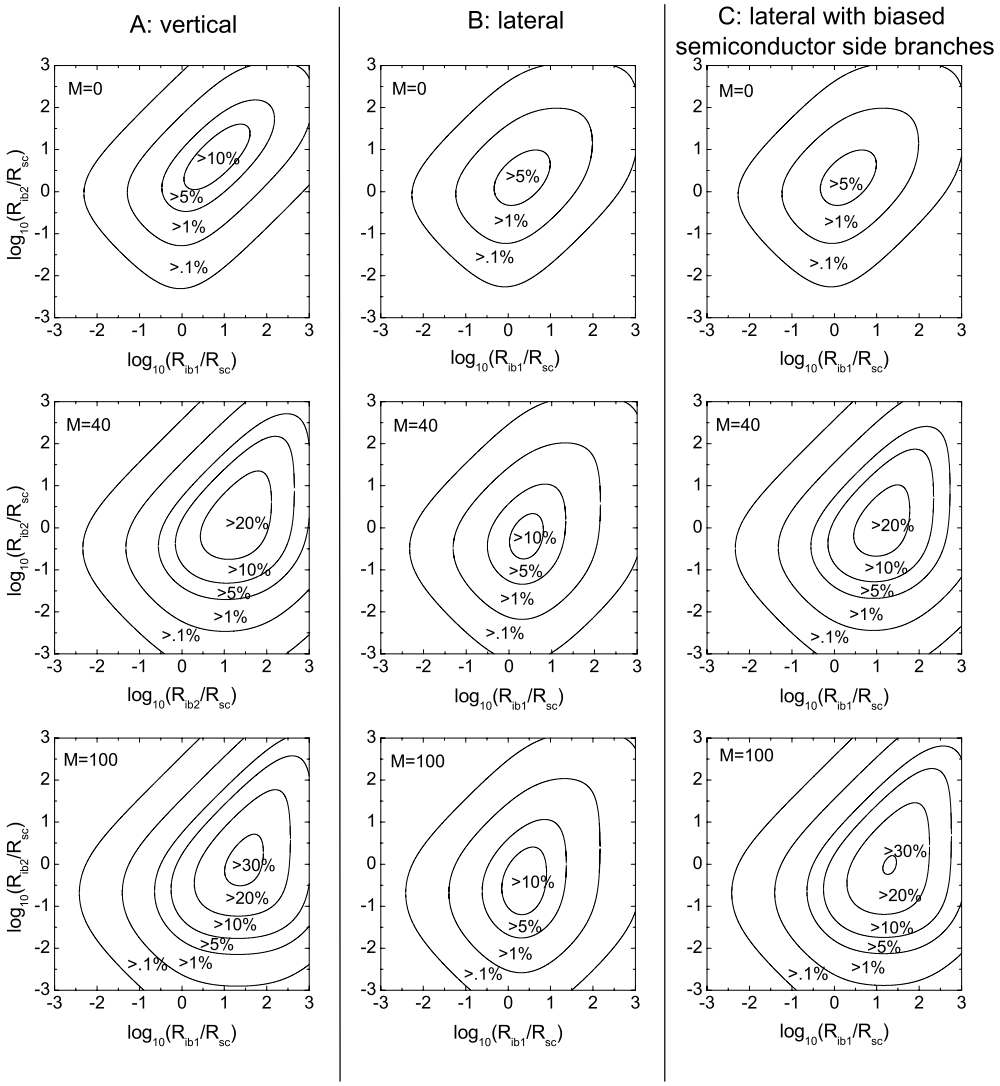

Figure 3. Contour plots of the magnetoresistance versus the injecting and detecting interface barrier resistances in units of the semiconductor resistance, $R_{\mathrm{ib1}}/R_{\mathrm{sc}}$ and $R_{\mathrm{ib2}}/R_{\mathrm{sc}}$. The magnetoresistance $(R_{\mathrm{ap}}-R_{\mathrm{p}})/R_0$ is calculated for fm/ib/sc/ib/fm structures in the vertical (column A) geometry, the lateral layout (column B), and the lateral geometry with biased semiconductor side branches (column C). For each geometry, three different electrical field parameters have been used, $M = 0, 40, 100$. In these calculations, we take $P_0 = 0.4$ and $\lambda/L = 5$.

the voltage drop over the device increases, due to higher interface barrier resistances, and the magnetoresistance drops down to zero.

Applying an electric field can enhance spin diffusion dramatically [33]. In the bottom two graphs of column A in figure 3, we show the influence of the electric field. Contour plots of the dependence of the magnetoresistance on both barrier resistances are shown for $M = 40$ and 100. Already for small fields, the range of R_{ib1} and R_{ib2} that results in a magnetoresistance above the detection limit, typically 1%, considerably increases. As long as the resistance

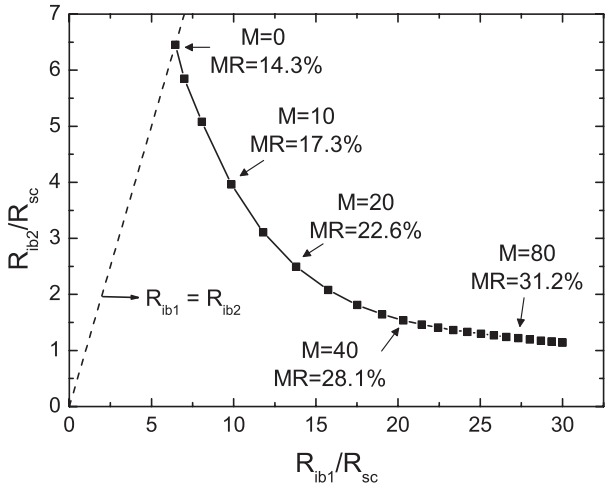

Figure 4. Calculation of the optimized magnetoresistance for different electric fields (represented by M) as a function of the injection and detection interface barrier resistances in units of the semiconductor resistance, for a vertical measurement geometry, where $P_0 = 0.4$ and $\lambda/L = 5$.

of the detection tunnel barrier is larger than the resistance of the injection tunnel barrier, the magnetoresistance increases monotonically with increasing M. As the electrical field is increased, the upstream and downstream spin diffusion lengths start to differ. Electrons follow a drift motion in addition to a random diffusive walk by which a higher spin accumulation is preserved over a longer distance, resulting in a higher magnetoresistance. Moreover, it can be seen in the figure that the measurement geometry is no longer symmetric upon interchanging the injection and detection sides. This shift of the optimum magnetoresistance will be explained in next paragraph.

For the vertical measurement geometry, we calculated for each value of the electric field the interface barrier resistances for which the magnetoresistance is maximum (see figure 4). For a small electric field, the device is symmetric and the injection and detection sides can be interchanged. Therefore, the maximum magnetoresistance corresponds to $R_{\mathrm{ib1}} = R_{\mathrm{ib2}}$. As the electrical field increases, the absolute value of the optimum injection barrier resistance (R_{tb1}) increases, and the absolute value of the optimum detection barrier resistance (R_{ib2}) decreases. This is a consequence of the fact that the upstream and downstream spin diffusion lengths start to differ ($\lambda_{\mathrm{u}} < \lambda < \lambda_{\mathrm{d}}$). As the injection barrier should match the downstream spin diffusion ($R_{\mathrm{ib1}} \sim 1/\lambda_{\mathrm{d}}$) and the detector barrier the upstream diffusion ($R_{\mathrm{ib2}} \sim 1/\lambda_{\mathrm{u}}$), optimum barrier values start to diverge.

In figure 5, the magnetoresistance is plotted as a function of the ratio between the spin flip length and the channel length for a set of parameters close to the optimum ratio ($R_{\mathrm{ib1}}/R_{\mathrm{sc}} = R_{\mathrm{ib2}}/R_{\mathrm{sc}} = 2$) and different values of the electric field. In absence of an applied voltage ($M = 0$), we observe that, as λ/L increases, the magnetoresistance increases monotonically. This is consistent with the fact that the probability of spin flip inside the semiconductor channel decreases with increasing ratio λ/L. For low rates of λ/L the magnetoresistance approaches zero, due to the lack of spin splitting. The upper limit $\lambda/L \to \infty$ corresponds to $P_0^2/(1 - P_0^2)$, half the magnetoresistance in the Julliere formula that would have been measured in a single tunnelling experiment between two ferromagnets. More interesting is that if an electric field is applied, the diffusion length splits up in the upstream and downstream diffusion lengths. This

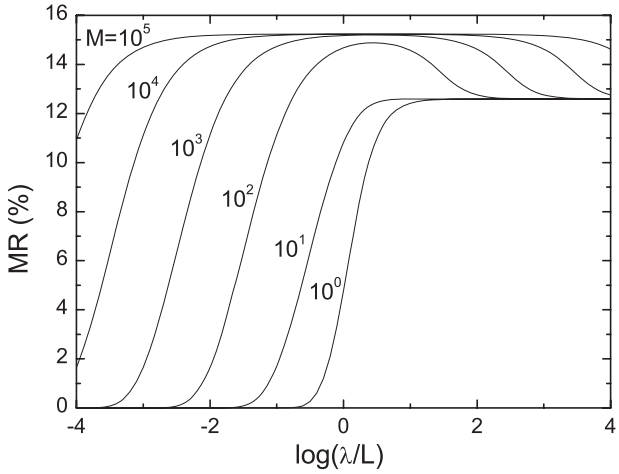

Figure 5. Magnetoresistance as a function of the ratio between the spin diffusion length λ and length of the semiconductor channel L for a vertical measurement geometry, and for different values of M, where $P_0 = 0.4$ and $R_{ib1}/R_{sc} = R_{ib2}/R_{sc} = 2$.

is only effective if the diffusion length is smaller than the semiconductor channel length, and thus the magnetoresistance increases rapidly for values of $\lambda/L < 1$. This offers the prospect of still a detectable spin splitting at larger separation of the injection and detection barriers or for smaller spin diffusion lengths. For instance, the magnetoresistance is still larger than 1% for $\lambda/L \approx 0.01$ for $M = 100$. The nonphysical maximum around $\lambda \approx L$ and the reduction of the magnetoresistance towards the asymptote can be attributed to the inclusion of the spin diffusion length in M (see equation (5)).

3.2. Magnetoresistance of a lateral measurement geometry

For a lateral measurement geometry, the magnetoresistance dependence on R_{ib}/R_{sc} is calculated with equation (11), and the results are shown figure 3(B), where M_3 is defined as M, and where M_4 and M_5 are set to zero. A horizontal comparison can be made between the vertical and lateral local measurement geometry for $M = 0$, 40 and 100. First let us investigate the dependence of the magnetoresistance at low bias ($M = 0$). We observe that the magnetoresistance is for every combination of interface barrier resistances smaller than for the vertical geometry. The optimum value is obtained now for $R_{ib1(2)}/R_{sc} \approx 2.1$ and thus shifted towards lower values of R_{ib}/R_{sc} as compared to the vertical devices ($R_{ib1(2)}/R_{sc} \approx 6.5$). Again, this numerical value heavily depends on the chosen parameters. The shift to lower $R_{ib1(2)}/R_{sc}$ is consistent with the fact that the total loss of spin information in the semiconductor is higher due to extra spin loss in the two semiconductor branches. This leads to a stronger coupling between the two channels, i.e. a higher equivalent spin flip conductance connecting the channels. As the maximum magnetoresistance is obtained when the barrier resistance matches the spin flip resistance, it is expected to be located at a lower $R_{ib1(2)}/R_{sc}$ ratio.

The contourplots for $M = 40$ and 100 in column B of figure 3 show the influence of the electric field for the lateral measurement geometry. If we consider for $M = 40$ for instance the 1% contour, the range of R_{ib1} and R_{ib2} considerably increases compared to the $M = 0$ graph. However, for $M = 100$, we observe that the magnetoresistance for certain interface barriers hardly changes. Together with the electric field in the semiconductor channel, the electric fields

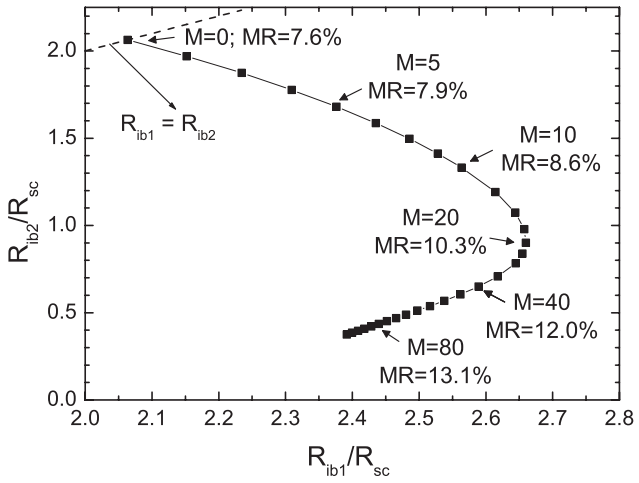

Figure 6. Calculation of the optimized magnetoresistance for different electric fields (represented by M) as a function of the injection and detection interface barrier resistances in units of the semiconductor resistance, for a lateral measurement geometry, where $P_0 = 0.4$ and $\lambda/L = 5$.

in the semiconductor side branches increase. The spin flip starts to be dominated by diffusion processes in these branches and the magnetoresistance saturates. Similar to the zero-field case, the magnetoresistance for lateral will always be lower than for vertical structures.

Analogously as for the vertical geometry, the optimum interface barrier resistance are calculated for different values of the electric field (see figure 6). The optimum injection barrier resistance (R_{ib1}) increases and the optimum detection barrier resistance (R_{ib2}) decreases for increasing electric fields up to $M = 20$. For larger electric fields, where $M > 20$, the optimum injection (detection) barrier resistance slowly drops towards the asymptotic value 2.4 (0.4). This value heavily depends on the chosen parameters ($P_0 = 0.4, \lambda/L = 5$). The optimum barrier resistance of the detector drops in the high-field regime because the influence on spin transport in the semiconductor is localized within the upstream length λ_{u} of the tunnel barrier. λ_{u} decreases with increasing field and becomes much shorter than L. Matching of both resistances according to $R_{\mathrm{ib1}} R_{\mathrm{ib2}}/R_{\mathrm{sc}}^2 \approx 1$ as shown in figure 3 leads to a maximum in $R_{\mathrm{ib1}}/R_{\mathrm{sc}}$. When the optimum injector barrier resistance no longer increases, the benefits of extra injection are balanced by the drawbacks of less detection, and therefore a maximum is found. Finally, when the spin-down length reaches the same value of the semiconductor channel length, further rise of M hardly affects the magnetoresistance and the optimum resistances no longer change.

Figure 7 shows the dependence of the magnetoresistance on the ratio between the spin flip length and the channel length, for $R_{\mathrm{ib1}} = R_{\mathrm{ib2}} = 2R_{\mathrm{sc}}$ (close to the optimum ratio), and for different electric fields. Analogously to the vertical geometry (see figure 5), we observe that as the λ/L ratio is increased, the magnetoresistance increases. However, an applied electric field yields only a minimal increase in magnetoresistance for the lateral geometry. The advantage of a higher drift velocity in between the electrodes (i.e. leading to higher magnetoresistance) is cancelled by a proportional increase of the drift velocity towards the outer ends of the semiconductor side branches (regions 4 and 5). More spin flip events in these regions reduce the existing spin accumulation in the semiconductor by which eventually the magnetoresistance saturates upon an increase of the electric field. In the next section, we will suggest a new measurement geometry which solves the fundamental problem of spin loss in the semiconductor side branches.

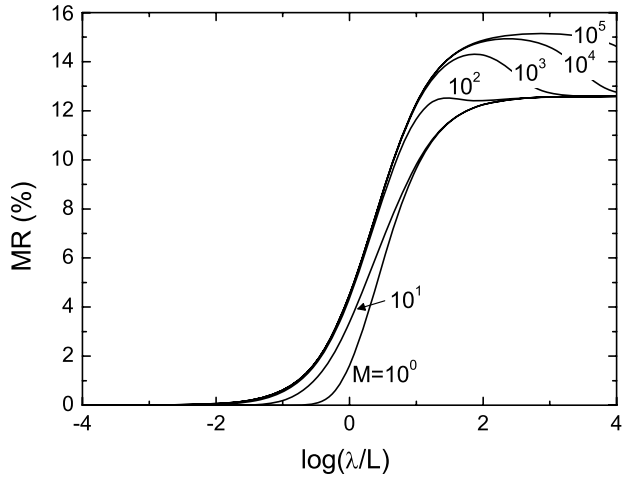

Figure 7. Expected magnetoresistance as a function of the ratio between the spin diffusion length λ and semiconductor channel length L for a lateral local measurement geometry, and for different values of M, where $P_0 = 0.4$ and $R_{ib1}/R_{sc} = R_{ib2}/R_{sc} = 2$.

3.3. Biasing the semiconductor side branches

In this section, we will discuss an improved layout to circumvent the extra spin flips in the semiconductor side branches. The much lower magnetoresistance value obtained in the lateral geometry compared to the vertical geometry originates from the extra spin flip processes in the two semiconductor side branches (region 4 and 5 in figure 2(a)). Moreover, the magnetoresistance improvements induced by the electric field are quenched in the lateral geometry due to inwardly pointed electric fields in the two side branches. Here we will show that the magnetoresistance can be improved if we apply an extra dc bias voltage to the detector electrode, with respect to the two side branches (see figure 8). The spin-dependent signal can be distinguished from the extra dc bias voltage by measuring in the ac mode. The electric field produced by this applied ac current has to be much smaller than the dc bias voltage. The dc electric field is assumed to be constant in the semiconductor, pointing outwards in both semiconductor branches and directed towards the detector electrode in the semiconductor transport channel (region 3). Large spin currents in the semiconductor side branches, which result in a large amount of spin flips, are now avoided, because drift in those regions will be minimal due to an opposite electric field. Therefore, relatively large detection spin currents and small spin currents in the semiconductor side branches will enhance the magnetoresistance. The given situation can be approximated if we substitute λ_u for λ in equation (11), which is equal to $M = M_3 = -M_4 = -M_5$ (M originates from the dc electric field). Analogously to the calculations for the lateral geometry the electrode resistances are assumed to be orders of magnitude smaller than the barrier resistances. Therefore, the R_1 and R_2 are set equal to zero, and the magnetoresistance corresponds to

$$\left(\frac{R_{ap} - R_p}{R_0}\right)_{bias} = \frac{4P_0^2}{(1-P_0^2)^2}\frac{R_{ib1}R_{ib2}}{R_{sc}(R_{ib1}+R_{sc}+R_{ib2})}\frac{(M^2+4)^{1/2}}{K_3} \times \frac{\cosh\left(\frac{M}{2K_3}\right)}{Q_1Q_2\exp\left(\frac{(M^2+4)^{1/2}}{2K_3}\right) - Q_3\exp\left(-\frac{(M^2+4)^{1/2}}{2K_3}\right)}$$

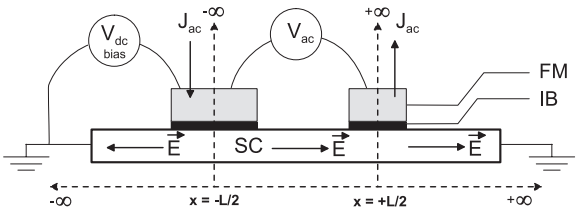

Figure 8. Cross section of the lateral spin-valve device in the ac measurement geometry with an extra dc bias voltage between the detector ferromagnet and the two semiconductor branches. A spin-polarized current is injected from region 1 into region 3 and detected at region 2. The electric field is assumed to be constant in the semiconductor, but the direction in the left semiconductor side branch is opposite to the direction in the right branch and the semiconductor channel.

with

$$Q_1 = \left[\frac{R_{\mathrm{ib1}}}{R_{\mathrm{sc}}(1-P_0^2)K_3}(-M+\sqrt{4+M^2})+1\right]$$
$$Q_2 = \left[\frac{R_{\mathrm{ib2}}}{R_{\mathrm{sc}}(1-P_0^2)K_3}(\sqrt{(4+M^2)}+1\right] \qquad (12)$$
$$Q_3 = \left[\frac{R_{\mathrm{ib1}}}{R_{\mathrm{sc}}(1-P_0^2)K_3}(-M)+1\right].$$

In column C of figure 3, the effect of tuning the electric field in the side branches on the magnetoresistance is shown for a broad range of injector and detector barrier resistances. Obviously, for zero bias ($M = 0$), the result for this new measurement geometry is identical to the lateral geometry. The expected magnetoresistance for the biased measurement geometry is already substantially improved for low electric fields. In comparison with the graphs of column B ($M = 40$ and 100), the matching regime is considerably broadened, confirming the robustness of the measurement geometry (e.g. consider the 5% contours of the graphs for $M = 40$ in columns B and C in figure 3). This can be an important step in realization of lateral semiconductor devices. For high fields ($M > 40$), the contour plots of the magnetoresistance will become identical to the vertical measurement geometry. The opposite electric fields in the semiconductor branches are so strong that any spin current is absent and the spin current layout of the vertical device is recovered. For $M \to \infty$ and $\lambda/L \to \infty$, the magnetoresistance is just limited to the maximum obtained for vertical devices, i.e.

$$\left(\frac{R_{\mathrm{ap}}-R_{\mathrm{p}}}{R_0}\right)_{\mathrm{bias,\,max}} = \frac{2P_0^2}{1-P_0^2}\frac{R_{\mathrm{ib1}}}{R_{\mathrm{sc}}+R_{\mathrm{ib1}}+R_{\mathrm{ib2}}}, \qquad (13)$$

which is the Julliere expression times a scaling factor, the ratio of the injection tunnel barrier over the total resistance [43]. As explained in section 3.1, the injection barrier resistance should match the downstream spin diffusion length, which is much shorter than the semiconductor channel length and is thus the critical parameter in equation (13).

To illustrate that the magnetoresistance increases already for low electric fields, we plotted the magnetoresistance as a function of M for $P_0 = 0.4$, $\lambda/L = 5$ and $R_{\mathrm{ib1}}/R_{\mathrm{sc}} = R_{\mathrm{ib2}}/R_{\mathrm{sc}} = 2$ together with the vertical and lateral local geometry (see figure 9). Already for $M \approx 10$, the magnetoresistance is almost equal to the values calculated for a vertical geometry. In this situation, only a few per cent of the increase in magnetoresistance between the biased and non-biased geometry can be attributed to the regular electric field dependent splitting of the diffusion lengths in the semiconductor channel. Again, for higher fields, the magnetoresistance converges to the vertical geometry and approaches the maximum described by equation (13).

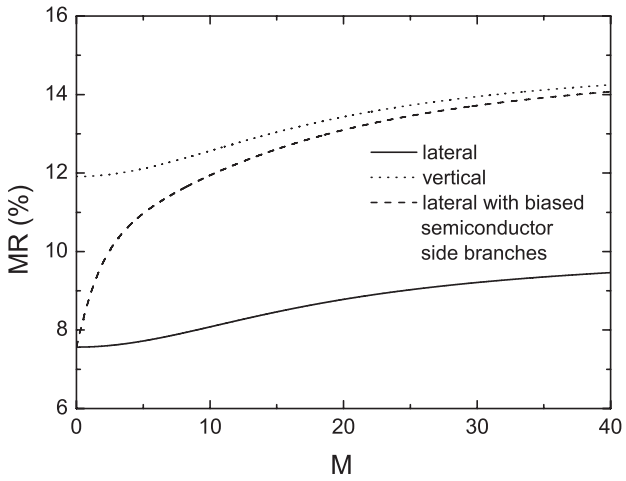

Figure 9. Dependence of magnetoresistance on the applied electrical field parameter (M), in a lateral measurement geometry with biased semiconductor side branches, where $P_0 = 0.4$, $\lambda/L = 5$ and $R_{ib1}/R_{sc} = R_{ib2}/R_{sc} = 2$.

For realistic devices, e.g. a semiconductor length of 1 μm and bias voltages of less than 3 mV, M is larger than 40 for all temperatures, and the magnetoresistance is already within 5% of magnetoresistance calculated for vertical structures ($R_{ib1}/R_{sc} = R_{ib2}/R_{sc} = 2$ and $\lambda/L = 5$).

Exploration of spin transport in materials with higher spin scattering probability (small spin diffusion length) or the development to longer spin channels (high L) is desired for the development of new spintronic components. In figure 10, we plotted the magnetoresistance as function of the ratio of the spin diffusion length and the semiconductor channel length. In absence of a bias, the curve is identical to the $M = 0$ curve of the lateral measurement geometry in figure 7. If the semiconductor side branches are biased with an extra dc electrical field, the magnetoresistance is approaching values obtained for the vertical device as shown in figure 5. From estimations based on figure 10, with a semiconductor channel length of 100 nm, and a biased electric field of a few mV per 10 nm, M can become as large as (1×10^9 m$^{-1} \times \lambda$), with λ in m for temperatures of 3 K. For spin diffusion lengths of the order of the mean free path, for which equations (9) and (11) are justified [13], a detectable magnetoresistance of at least 1% should be observed, which is very promising for experimental devices. For devices operating at room temperature, M has a maximum value of (4×10^7 m$^{-1} \times \lambda$), and the minimum spin diffusion length for observing magnetoresistance can still be as short as 50 nm.

Although there has been significant progress in recent years in achieving efficient electrical semiconductor spin-valves, up to now different experiments show only marginal effects. Koo *et al* [44] demonstrated full electrical spin injection and detection in InAs quantum wells with an observed magnetoresistance as small as 0.029%. Saha *et al* [30] reported magnetoresistance of epitaxially grown MnAs/GaAs lateral spin-valves of 3.6%, which is according to the authors much higher as predicted on the basis of only diffusive transport and using a conservative value for the spin polarization. Consistent with our calculations, they measure a decreasing magnetoresistance with the channel length. The magnetoresistance increases with current, which may be similar to what is shown in figure 7 for electric fields equivalent to their device operation. However, the increase of magnetoresistance can also be explained by an enhancement of spin injection efficiency due to narrower depletion widths. Spin-valve magnetoresistance effects of 0.001% have been measured in lateral ferromagnet–

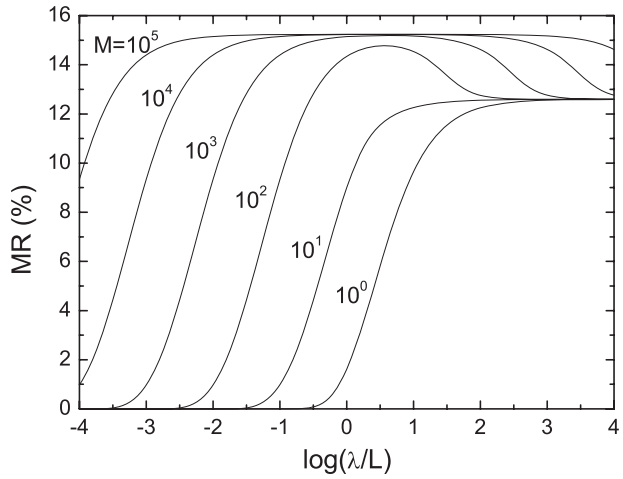

Figure 10. Expected magnetoresistance as a function of the ratio between the spin diffusion and semiconductor channel length for a lateral measurement geometry with biased semiconductor side branches (different values of M), where $P_0 = 0.4$ and $R_{ib1}/R_{sc} = R_{ib2}/R_{sc} = 2$.

semiconductor devices by Lou *et al* [10]. They irrefutably proved the electrical detection of spin transport by using the Hanle effect to suppress the nonlocal signal and by simultaneously optically investigation of spin accumulation in the channel via the Kerr effect. Their measured effect is, however, significantly lower than our optimized predictions in this paper.

Substantial differences between our calculations and experimental results might be the result of the use of non-optimized parameters in these experiments (channel length, spin diffusion length, bias voltage, and interface and channel resistances). Additionally, we would like to mention that the nonlocal magnetoresistance, as commonly exploited, is half the magnetoresistance predicted in the local geometry. Further reductions to lower magnetoresistance can be justified, because our quasi-two-dimensional solutions do not include current spreading or current crowding, and assume perpendicular injection and detection at only a single point [32]. Insertion of highly doped layers to locally suppress the width of the Schottky barrier influences the carrier concentration, and can partially lead to depolarization of the carriers along the current path. Carriers extracted from above the Fermi level will be subject to small negative built-in electric fields. The spin accumulation, and thereby the magnetoresistance, reduces when the negative electric field extends over a distance comparable to the spin diffusion length. Finally, impurities at the interfaces or Rashba effects in the semiconductor interface regions, where an electric field perpendicular to the current transport can be present, possibly introduce additional spin flip channels. However, the relation between these scattering effects that govern the mobility and the spin relaxation mechanisms may be quite subtle.

4. Conclusions

From the Poisson and diffusion equation, a general drift–diffusion equation was derived by Yu and Flatté [33], valid for metals and semiconductors. For a vertical device, a lateral device and a lateral device with biased semiconductor side branches, we have given an analytical expression for the magnetoresistance. Subsequently, for these geometries the role of the elementary transport parameters (resistance, spin diffusion length and electric field) on the

magnetoresistance is examined. If the electric field (applied bias voltage) exceeds a certain critical value in semiconductors, there will be two distinct spin diffusion lengths, i.e. an upstream and downstream spin diffusion length. This effect can enhance the spin diffusion and magnetoresistance dramatically. Via an extra bias voltage, electric fields can be created in the semiconductor side branches such that the magnetoresistance closely approaches values of vertical devices. This improvement of spin transport could be used to measure devices with longer channel lengths or smaller spin flip lengths due to, for example, higher temperatures or different materials for spin transport.

Acknowledgment

This work was supported by the Dutch Technology Foundation (STW) via NWO VICI-grant 'Spintronics'

References

[1] Wolf S, Awschalom D D, Buhrman R A, Daughton J M, van Molnar S, Roukes M L and Treger D M 2001 *Science* **194** 1488
[2] Leuenberger M N, Loss D, Poggio M and Awschalom D D 2002 *Phys. Rev. Lett.* **89** 207601
[3] Ney A, Pampuch C, Koch R and Ploog K H 2003 *Nature* **425** 485
[4] Kikkawa J M and Awschalom D D 1999 *Nature* **397** 139
[5] Fiederling R, Reuscher G, Ossau W, Schmidt G, Waag A and Molenkamp L W 2000 *Nature* **402** 787
[6] Ohno Y, Young D K, Beschoten B, Matsukura F, Ohno H and Awschalom D D 1999 *Nature* **402** 790
[7] Motsnyi V F, de Boeck J, Das J, Van Roy W, Borghs G, Goovaerts E and Safarov V I 2002 *Appl. Phys. Lett.* **81** 265
[8] Crooker S A, Furis M, Lou X, Adelmann C, Smith D L, Palmstrøm C J and Crowell P A 2005 *Science* **309** 2191
[9] Crooker S A and Smith D L 2005 *Phys. Rev. Lett.* **94** 236601
[10] Lou X, Adelmann C, Crooker S A, Garlid E S, Zhang J, Madhukar Reddy K S, Flexner S D, Palmstrøm C J and Crowell P A 2007 *Nat. Phys.* **3** 197
[11] Johnson M and Silsbee R H 1987 *Phys. Rev.* B **35** 4959
[12] Valet T and Fert A 1993 *Phys. Rev.* B **48** 7099
[13] Penn D R and Stiles M D 2005 *Phys. Rev.* B **72** 212410
[14] Schmidt G, Ferrand D, Molenkamp L W, Filip A T and van Wees B J 2000 *Phys. Rev.* B **62** R4790
[15] Ren J F, Fu J Y, Liu D S, Mei L M and Xie S J 2005 *J. Appl. Phys.* **98** 0074503
[16] Rashba E I 2000 *Phys. Rev.* B **62** R16267
[17] Fert A and Jaffrès H 2001 *Phys. Rev.* B **64** 184420
[18] Khaetskii A, Egues J C, Loss D, Gould C, Schmidt G and Molenkamp L W 2005 *Phys. Rev.* B **71** 235327
[19] Agrawal S, Jalil M B A and Teo K L 2005 *J. Appl. Phys.* **97** 103907
[20] Dery H, Cywiński Ł and Sham L J 2006 *Phys. Rev.* B **73** R041306
[21] Dery H, Cywiński Ł and Sham L J 2006 *Phys. Rev.* B **73** R161307
[22] Cywiński Ł, Dery H and Sham L J 2006 *Appl. Phys. Lett.* **89** 042105
[23] McGuire J P, Ciuti C and Sham L J 2004 *Phys. Rev.* B **69** 115339
[24] Yu Z G and Flatté M E 2002 *Phys. Rev.* B **66** R201202
[25] D'Amico I 2004 *Phys. Rev.* B **69** 165305
[26] Van Roy W, Van Dorpe P, De Boeck J and Borghs G 2006 *Mater. Sci. Eng.* B **126** 155
[27] Filip A T, Schoonus J J H M, Swagten H J M, Koopmans B, De Jonge W J M, Karouta F, Geluk E J, Van Roy W and De Boeck J 2005 *J. Supercond.* **18** 379
[28] Van Dorpe P, Vanheertum R, Boukari H, Van Roy W and Borghs G 2006 *J. Appl. Phys.* **99** 08S702
[29] Schoonus J J H M, Kurnosikov O, Swagten H J M, Koopmans B, Geluk E J, Karouta F, Van Roy W and Borghs G 2006 *Phys. Status Solidi* c **3** 4176
[30] Saha D, Holub M, Bhattacharrya and Liao Y C 2006 *Appl. Phys. Lett.* **89** 142504
[31] Schmidt G, Gould C, Grabs P, Lunde A M, Richter G, Slobodskyy A and Molenkamp L W 2004 *Phys. Rev. Lett.* **92** 226602
[32] Vanheertum R, Van Dorpe P, Borghs G and Van Roy W 2006 *Phys. Status Solidi* c **3** 4172
[33] Yu Z G and Flatté M E 2002 *Phys. Rev.* B **66** 235302

[34] Malajovich I M, Berry J J, Samarth N and Awschalom D D 2001 *Nature* **411** 770
[35] D'Amico I and Vignale G 2001 *Europhys. Lett.* **55** 566
[36] Kikkawa J M and Awschalom D D 1998 *Phys. Rev. Lett.* **80** 4313
[37] Flensberg K, Jensen T S and Mortensenm N A 2001 *Phys. Rev.* B **64** 245308
[38] Jedema F J, Nijboer M S, Filip A T and Van Wees B J 2003 *Phys. Rev.* B **67** 085319
[39] Van Son P C, Van Kempen H and Wyder P 1987 *Phys. Rev. Lett.* **58** 2271
[40] Upadhyay S K, Palanisami A, Louie R N and Buhrman R A 1998 *Phys. Rev. Lett.* **81** 3247
[41] Jiang X, Wang R, Shelby R M, Macfarlane R M, Bank S R, Harris J S and Parkin S S P 2005 *Phys. Rev. Lett.* **94** 056601
[42] Braden J G, Parker J S, Xiong P, Chun S H and Samarth N 2003 *Phys. Rev. Lett.* **91** 056602
[43] Filip A T, LeClair P, Smits C J P, Kohlhepp J T, Swagten H J M and De Jonge W J M 2002 *Appl. Phys. Lett.* **81** 1815
[44] Koo H C, Yi H, Chang J, Han S-H, Jung D, Huh S-G and Eom J 2007 *Appl. Phys. Lett.* **90** 022101